Decentralized Short-Term Voltage Control in Active Power Distribution Systems

Changsen Feng, Zhiyi Li, *Graduate Student Member, IEEE*, Mohammad Shahidehpour, *Fellow, IEEE*, Fushuan Wen, Weijia Liu, and Xiaolei Wang

***Abstract*—With increasing utilizations of distributed energy resources and smart energy apparatuses, power distribution systems are undergoing a transition from passive to active networks, which challenges distribution system operators in many aspects of energy management and system control. In this paper, a short-term control strategy for active power distribution systems is proposed to regulate voltages into statutory ranges. The voltage control strategy is modeled as a convex optimization problem by applying a second-order cone relaxation. After the network decomposition, the alternating direction method of multipliers is employed to solve the established optimization model in a decentralized mode. Finally, the IEEE 33-bus and 123-bus test systems are employed to demonstrate the performance of the proposed voltage control strategy in active power distribution systems.**

***Index Terms*—Active power distribution system, decentralized optimization, hierarchical control framework, second-order cone programming.**

I. Introduction

RENEWABLE energy-based distributed generations and storage units are commonly termed as distributed energy resources (DERs). Currently, the increasing penetration of DERs, the implementation of smart distribution technologies such as advanced metering/monitoring infrastructure, and the adoption of smart appliances are major driving forces for a transition to active power distribution systems (APDS) [1]. The frequent variations in DER power outputs could have negative impacts on the APDS voltage profile, especially for the situations with high resistance-to-reactance ratios in distribution lines [2]. Therefore, voltage control is a vital issue in implementing effective coordination of DERs for enhancing the power quality in APDS.

Manuscript received April 30, 2016; revised August 20, 2016 and December 26, 2016; accepted January 31, 2017. Date of publication February 2, 2017; date of current version August 21, 2018. This work was supported in part by the National Natural Science Foundation of China under Grant 51477151 and Grant U1509218, and in part by the National High Technology Research and Development Program of China 863 Program under Grant 2015AA050202. Paper no. TSG-00577-2016.

C. Feng, W. Liu, and X. Wang are with the School of Electrical Engineering, Zhejiang University, Hangzhou 310027, China (e-mail: fengchangsen@126.com; liuweijiamarcel@gmail.com; sunflowerxiaolei@qq.com).

Z. Li and M. Shahidehpour are with the Galvin Center for Electricity Innovation, Illinois Institute of Technology, Chicago, IL 60616 USA (e-mail: zhiyi.li@hawk.iit.edu; ms@iit.edu).

F. Wen is with the School of Electrical Engineering, Zhejiang University, Hangzhou 310027, China, and also with Universiti Teknologi Brunei, Bandar Seri Begawan BE1410, Brunei (e-mail: fushuan.wen@gmail.com).

Color versions of one or more of the figures in this paper are available online at http://ieeexplore.ieee.org.

Digital Object Identifier 10.1109/TSG.2017.2663432

Hierarchical voltage control strategies are widely adopted in power system operation [3]. More specifically, the primary-level control provides fast control actions to handle local voltage perturbations; the secondary-level control coordinates reactive power regulators to improve regional voltage levels; the tertiary-level defines voltage set-points by determining the optimal power flow in APDS [4], [5]. However, higher penetrations of DERs impose great challenges on distribution system operators (DSO) to maintain voltages within predefined ranges. In this regard, DERs seldom provide voltage support mainly because DSOs normally operate them with fixed power factors which limit the DER integration into APDS [6]. Typical voltage control measures such as on-load tap changing, voltage regulation and shunt capacitor adjustment are effective in mitigating slow (e.g., hourly) violations. However, the lifetime of these mechanical devices would be substantially reduced if they are manipulated frequently to offset voltage violations resulting from quick (e.g., minutes) DER power productions [7], [8]. Thus, DSOs could consider DER potentials for mitigating frequent voltage violations, and this represents a unique feature of voltage control in APDS. However, the implementation of a wide variety of control devices and state-of-the-art strategies make voltage control more complex, corresponding to a larger optimization problem [9].

The voltage control problem in APDS has been addressed in some existing publications. Reference [10] offers comprehensive guidelines for DG inverters to participate in the coordinated voltage and reactive power control. Reference [2] proposed a method to enhance the DER utilization for voltage control. A two-stage robust optimization model is proposed in [11] for reactive power optimization which coordinates discrete and continuous reactive power compensators to avoid any voltage violations in variable wind power output. Reference [12] developed a centralized control scheme based on model predictive control to correct voltages out of assigned ranges by solving a multi-step quadratic programming problem. Reference [13] introduced an iterative heuristic algorithm to improve the performance of multi-phase distribution networks by properly placing and sizing DERs and capacitors. The cited publications employ a centralized mode.

The traditional voltage control model was not considered in a convex programming problem, due to nonconvex power flow equations, of which the global optimal solution was difficult to attain. The nonconvex equations can however be relaxed, convexified by the cone relaxation technique, and

transformed into a second-order cone (SOC) form [14]–[18]. Reference [15] showed that the conic relaxation usually offers a small gap with the original power flow solution in most distribution systems. Besides, the conic relaxation technique is widely used in the existing literature. For example, the reactive power control is formulated as an optimal power flow problem in [17] and applied to the resulting nonconvex problem using the SOC relaxation under sufficient conditions. Compared with [17], [18] gives less restrictive and sufficient conditions under which the SOC relaxation is exact. Different from the previous works, our proposed model in this paper is amenable for a distributed system implementation.

Conventionally, distribution systems are centrally controlled by DSO. However, for geographically dispersed DERs, centralized approaches require significant investments for the implementation of control centers and relevant communication infrastructures. Moreover, the data storage in DSO carries the risk of leaking users' privacy, let alone the unavoidable single point of failure [19]. Thus, it is desirable to coordinate DERs and controllable loads in a distributed way. Advances in microprocessor chip designs have made the decentralized control quite feasible. More importantly, the distributed method can greatly reduce the calculation time compared with the centralized manner.

There are numerous publications on the distributed optimization and control of power systems. For example, the work in [20] provides a distributed control scheme to guarantee all photovoltaic (PV) systems to run at the same output ratio. Reference [21] proposes a decentralized method of voltage control which uses the self-information without any external communication. Distributed primal-dual subgradient algorithms in [22] are devised and then adopted in the optimal dispatch model of virtual power plants [23]. There are also many publications about distributed optimization based on ADMM. References [24] and [25] propose a decentralized method to attain a tie-line scheduling considering uncertainties. The work in [26]–[28] relaxes the OPF into SDP exactly under some conditions and provides a distributed optimization method for multi-phase unbalance networks. Different from existing research work, the method proposed in this paper has self-healing capability which embodies plug and play options.

The contributions of this paper are threefold. First, different from the traditional voltage control model, a coupled active-reactive power optimization model based on a hierarchical control architecture is presented which can implement the potential benefits of DERs. Meanwhile, the second-order cone relaxation technique is employed to reformulate the model. Secondly, a distributed solution method based on ADMM is developed which merely requires the exchange of local information among neighboring control areas. Thirdly, this work provides a qualitative analysis about the robust performance of the proposed method through comparison studies between two modes. The proposed method can accommodate random communication failures to a certain degree, and hence has better self-healing capability. Moreover, the difference between this work and [16] which represents a part of the contribution is that the proposed method can adapt to frequent changes of topological structures and accommodate any number of devices given that a high-level integration of plug and play devices into a distribution system.

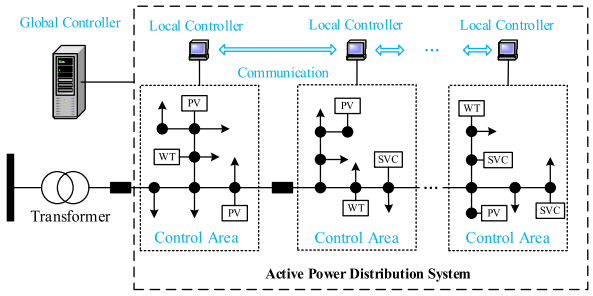

Fig. 1. Hierarchical and multi-area control architecture.

The remainder of the paper is organized as follows: Section II introduces hierarchical and multi-area control architectures. Section III formulates the voltage control as an optimization problem and convexifies it through the conic relaxation. Section IV models each fundamental device in APDS. Section V proposes a decentralized solution method based on ADMM. The performance of the proposed approach is demonstrated in Section VI. Conclusions together with future work are given in Section VII.

II. Hierarchical Multi-Area Voltage Control

As massive integrations of DERs and controllable loads into APDS are considered, it is impractical for control centers to directly regulate each device in order to attain the global optimum. Thus, a hierarchical and multi-area control framework is preferably established for voltage control in this situation [29]. The proposed architecture is composed of two key aspects. First, the original APDS is divided into several layers according to the line voltage level. Secondly, each subdivision layer is further divided into several small-scale regions at the same voltage level [30]. Under this architecture, as shown in Fig. 1, voltage control can be implemented by a bi-level programming problem in which the upper-level determines the global voltage control and the lower-level is in charge of the regional voltage control.

On the one hand, the upper-level voltage control would provide a system-wide energy management, in which the decision variables (e.g., settings of transformer taps and shunt capacitor banks) remain fixed in a longer time scale (e.g., hourly). Given that the decision variables are usually discrete in nature, the upper-level model is a mixed-integer programming problem. As shown in Fig. 2, once the upper-level decisions are made, the lower-level voltage control is thereupon implemented. Note that the lower-level voltage control focuses on a shorter time scale (e.g., minute). The relevant decision variables include settings of static Var compensators (SVCs) and DGs' coupling inverters, as well as the amount of controllable loads, which are usually continuously adjustable with better dynamic and adaptive performances. We assume that the decision variables in the upper-level model have been determined in some way and more details are available in [6], [8], [11], and [12]. The focus of this paper is on the lower-level voltage control since

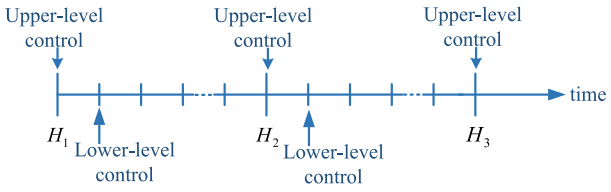

Fig. 2. Temporal decomposition and coordination of hierarchical voltage control.

voltage security in APDS is severely affected by variable DER outputs in a short time scale.

The lower-level voltage control (abbreviated as voltage control hereinafter) can be parallelized with a multi-area control structure. The control area in APDS is defined as a sub-network with relatively complete topology which can eliminate regional voltage deviations by introducing measures such as load transfers and Var compensations. A DG or a controllable load can be deemed as a smallest control area while feeders, which are interconnected by tie switches, can be seen as a largest control area. In general, a 10 kV distribution system can be divided into several control areas according to their geographic and topology structures: 1) a loop switch or sectionalizing switch defines the bound of the control area; 2) the area between two sectionalizing switches or between the sectionalizing switch and the end of the line is viewed as a control area if it has controllable devices.

III. Mathematical Formulation

A. Objective Function

In fact, there exists a complex coupling relationship between the voltage profile and network losses. If only the network loss is minimized, it may result in unpredictable deviations of voltage magnitudes. Thus, in order to evaluate the overall system conditions comprehensively, both network losses and nodal voltage deviations are considered.

The total network loss is defined as the sum of individual branch losses, and formulated as

$$F_1 = \sum_{(i,k)\in E} r_{ik} \times \frac{P_{ik}^2 + Q_{ik}^2}{|V_i|^2} \tag{1}$$

where E is the set of directed branches in APDS; P_{ik} and Q_{ik} are active and reactive power flow in branch (i,k), respectively; V_i is the voltage magnitude at bus i and r_{ik} is the distribution line resistance.

The accumulated nodal voltage deviations can be defined as

$$F_2 = \sum_{i\in B} \left(\frac{V_i - V_i^{ref}}{\bar{V}_i - \underline{V}_i} \right)^2 \tag{2}$$

where B is the set of terminal buses in APDS; $\bar{V}_i$ and $\underline{V}_i$ respectively denote upper and lower voltage limits at bus i, while V_i^{ref} represents the reference value. In addition, if the voltage magnitude of a critical bus is required to be fixed at its reference value, the upper and the lower bounds are set at the same values, thereby leading voltage deviations to zero.

A comprehensive evaluation index F is proposed as the objective to be minimized [31], and formulated as

$$F = w_1 F_1 / F_1^0 + w_2 F_2 / F_2^0 \tag{3}$$

where F_1^0 and F_2^0 are the normalization factors calculated from historical operation data; w_1 and w_2 are the predefined non-negative weights, and $w_1 + w_2 = 1$.

B. Constraints

The constraints in the optimization model include power flow equations, and limits on nodal voltage magnitudes and branch flows.

Conventionally, power flow equations are formulated as

$$\begin{cases} P_i = V_i \sum_{k\in\pi(i)} V_k (G_{ik}\cos\theta_{ik} + B_{ik}\sin\theta_{ik}) \\ Q_i = V_i \sum_{k\in\pi(i)} V_k (G_{ik}\sin\theta_{ik} - B_{ik}\cos\theta_{ik}) \end{cases}, \quad \forall i \in B \tag{4}$$

where G_{ik} and B_{ik} are the real and imaginary parts of the nodal admittance matrix, respectively; $\pi(i)$ is the set of neighboring buses of bus i. Note that (4) is based on bus injections which can be represented in the branch-flow model [14]:

$$\begin{cases} P_{ik} = \sum_{m:(m,i)\in E} P_{im} + r_{ik}\frac{P_{ik}^2+Q_{ik}^2}{|V_i|^2} - P_i \\ Q_{ik} = \sum_{m:(m,i)\in E} Q_{im} + x_{ik}\frac{P_{ik}^2+Q_{ik}^2}{|V_i|^2} - Q_i \\ |V_k|^2 = |V_i|^2 - 2(r_{ik}P_{ik} + x_{ik}Q_{ik}) + \left(r_{ik}^2 + x_{ik}^2\right)\frac{P_{ik}^2+Q_{ik}^2}{|V_i|^2} \end{cases}, \quad \forall (i,k) \in E \tag{5}$$

where x_{ik} denotes the reactance of branch (i,k), and the active P_i and reactive Q_i injections at bus i are given by

$$\sqrt{\frac{P_{ik}^2 + Q_{ik}^2}{|V_i|^2}} \le I_{ik}^{\max}, \quad \forall (i,k) \in E \tag{6}$$

where p_i^g and q_i^g denote the active and reactive power generations by the DG at bus i, respectively; p_i^c and q_i^c represent active and reactive power consumptions at bus i, respectively; q_i^{SVC} is the reactive power delivered by SVC at bus i; the reactive power generated by the shunt capacitor bank at bus i is represented by $q_i^{sc}|V_i|^2$ in which q_i^{sc} is the reactive power generation at the nominal voltage (i.e., $|V_i|$=1). Additionally, the power output of DGs or SVCs cannot violate the respective upper and lower limits, which could be due to capacity limits or security considerations. More specifically, the DG power outputs at bus i conform to:

$$\begin{cases} 0 \le p_i^g \le \bar{p}_i^g \\ \underline{q}_i^g \le q_i^g \le \bar{q}_i^g \end{cases}, \quad \forall i \in B \tag{7}$$

while the power output of a SVC is constrained by

$$\underline{q}_i^{SVC} \le q_i^{SVC} \le \bar{q}_i^{SVC}, \quad \forall i \in B \tag{8}$$

where $\underline{q}_i^{SVC}$ and $\bar{q}_i^{SVC}$ are the lower and upper limits of reactive power provided by SVC, respectively.

In fact, the nodal voltage magnitude is regulated in order to maintain the power delivery, and constrained by

$$\underline{V}_i \le V_i \le \bar{V}_i, \quad \forall i \in B \tag{9}$$

where the limits are $\underline{V} = (1-\varepsilon)V^{ref}$ and $\bar{V} = (1+\varepsilon)V^{ref}$. According to [32], ε is usually set to 0.05. Besides, branch

flows should be within the corresponding thermal limits. In other words, the line current cannot exceed its maximum:

$$\sqrt{\frac{P_{ik}^2+Q_{ik}^2}{|V_i|^2}} \le I_{ik}^{\max},\ \forall (i,k)\in E. \tag{10}$$

C. Second-Order Cone Relaxation

Now we can form our proposed model for the optimal voltage control in APDS, which minimizes the objective function (3) and respecting (5)-(10). However, this model pertains to a nonconvex programming problem, which is technically intractable for a global optimal solution with the fast-increasing number of decision variables resulting from extensive DER penetrations into APDS. The nonconvex power flow can be convexified by the SOC relaxation technique [14].

The relaxation performed on the branch-flow-based power flow equation is shown as follows. At first, two sets of artificial variables are introduced as

$$l_{ik} = \frac{P_{ik}^2+Q_{ik}^2}{|V_i|^2},\ \forall (i,k)\in E \tag{11}$$

$$v_i = V_i^2,\ \forall i\in B \tag{12}$$

Substituting (11) and (12) into (5) yields:

$$\begin{cases} P_{ik} = \sum_{m:(i,m)\in E} P_{im} + r_{ik}l_{ik} - P_i \\ Q_{ik} = \sum_{m:(i,m)\in E} Q_{im} + x_{ik}l_{ik} - Q_i \\ v_k = v_k - 2(r_{ik}P_{ik}+x_{ik}Q_{ik}) + \left(r_{ik}^2+x_{ik}^2\right)l_{ik} \end{cases},\ \forall (i,k)\in E \tag{13}$$

Then relaxing (11) into an inequality results in:

$$l_{ik} \ge \frac{P_{ik}^2+Q_{ik}^2}{v_i},\ \forall (i,k)\in E \tag{14}$$

which can be rewritten in the standard form of SOC:

$$\left\| \begin{matrix} P_{ik} \\ Q_{ik} \\ (l_{ik}-v_i)/2 \end{matrix} \right\|_2 \le \frac{l_{ik}+v_i}{2},\ \forall (i,k)\in E \tag{15}$$

where $\|\cdot\|_2$ is the Frobenius norm.

Such SOC relaxations are exact for most power distribution systems [15]. Besides, when V_i^2 is replaced by v_i, the accumulated nodal voltage deviations in (2) are further transformed into the following form for ease of calculation:

$$F_2 = \sum_{i\in B}\left(\frac{v_i - v_i^{ref}}{\bar{V}_i^2 - \underline{V}_i^2}\right)^2 \tag{16}$$

where $v^{ref} = (V^{ref})^2$.

IV. Network Decomposition and Component Modeling

In this section, network decomposition is addressed so as to solve the proposed SOCP in a decentralized way and provide the model for each fundamental component in APDS.

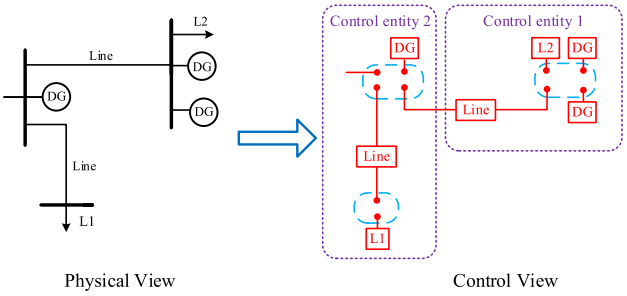

Fig. 3. Distributed model for distribution systems.

A. Networked Control Entities

Inspired by the common information model [33], APDS can be decomposed into components with terminals and then aggregated into control entities so that APDS can be seen as a system of networked control entities as shown in Fig. 3. A set of terminals, which are associated with the same bus, makes up a junction. Here the terminal represents electric variables such as complex power and voltage; the component includes DERs, loads and distribution lines.

A is a finite set of the control entity a. J is a finite set of decoupled junctions j. T is a finite set of terminals t, which is partitioned into subsets in terms of the control entity A or J in terms of junctions. Each element in A and J (i.e., a_d and j_d) contains all the associated terminals of cardinality $|a_d|$ and $|j_d|$. The following conditions are always met:

$$\bigcup_{a_d\in A} a_d = \bigcup_{j_d\in J} j_d = T \tag{17}$$

$$\bigcap_{a_d\in A} a_d = \bigcap_{j_d\in J} j_d = \emptyset \tag{18}$$

Each terminal has an associated complex power S_t and voltage magnitude V_t. The set of complex power and voltage magnitude associated with the control entity a is denoted by $S_a=\{S_t|t\in a\}$ and $V_a=\{V_t|t\in a\}$, respectively. Here, S_a is a two-dimensional matrix and V_a is an one-dimensional array. The set associated with the junction j is denoted by $S_j=\{S_t|t\in j\}$ and $V_j=\{V_t|t\in j\}$, respectively.

During each period, the network must respect the Kirchhoff's law, which satisfies the power balance and voltage magnitude consistency at each junction. Define the average net power imbalance $\bar{S}_t$ and voltage magnitude residual $\tilde{V}_t$ as:

$$\bar{S}_t = \frac{1}{|j|}\sum_{t\in j} S_t \tag{19}$$

$$\tilde{V}_t = V_t - \frac{1}{|j|}\sum_{t\in j} V_t = V_t - \bar{V}_t \tag{20}$$

Thus, the optimization model is written as:

$$(\mathbf{P1})\ \min \sum_{a\in A} F_a(S_a, V_a) \tag{21a}$$

$$s.t.\ \ \bar{S}=0,\ \tilde{V}=0 \tag{21b}$$

$$S\in \mathbf{S}\ and\ V\in \mathbf{V} \tag{21c}$$

where $\mathbf{S}$ and $\mathbf{V}$ are the local constraints of decision variables. For clarity, subscript t is omitted hereinafter except noted.

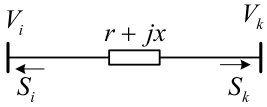

Fig. 4. Distribution line model.

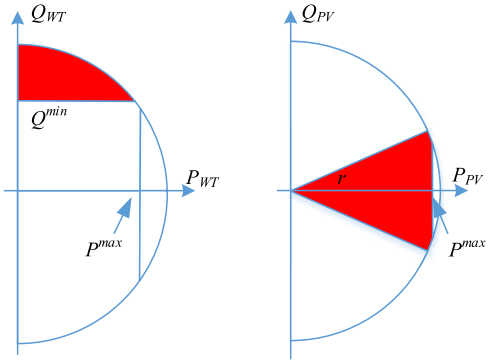

(a) WT (b) PV

Fig. 5. The P-Q plane of an inverter for WT and PV.

B. Modeling Distribution Line

A distribution line, as shown in Fig. 4, is regarded as a two-terminal device with two complex power outflows $\dot{S}_i$ and $\dot{S}_k$. $\dot{Z}_{ik}$ is the impedance of line between nodes i and k, and represented by $\dot{Z}_{ik} = r_{ik} + j \cdot x_{ik}$. The set of branch-flow equations is then transformed as ($\forall (i,k) \in E$):

$$S_i + S_k = -l_{ik} \cdot Z_{ik} \tag{22}$$

$$v_k = v_i + l_{ik} * \|Z_{ik}\|_2^2 + 2S_i * Z_{ik}^{\mathrm{T}} \tag{23}$$

$$\underline{V}_i^2 \le v_i \le \bar{V}_i^2, \underline{V}_k^2 \le v_k \le \bar{V}_k^2 \tag{24}$$

$$l_{ik} \le \left(I_{ik}^{\max}\right)^2 \tag{25}$$

where $S_{i(k)} = [\mathrm{Re}(\dot{S}_{i(k)}), \mathrm{Im}(\dot{S}_{i(k)})]$ and $Z_{ik} = [\mathrm{Re}(\dot{Z}_{ik}), \mathrm{Im}(\dot{Z}_{ik})]$. More specifically, (22) captures the power balance along this branch; (23) describes the relationship between the associated terminal voltages; (24) represents the voltage magnitude limits; and (25) describes the thermal flow limit.

C. Modeling DERs

Here several representative DERs will be modeled including a wind turbine, a PV system, and an electric storage system (ESS).

1) Wind Turbine and PV System: Considering the inevitable prediction error of active power generated by a wind turbine and a PV system, we set the forecast value as the upper limit of active power $\bar{P}_{DG}$, while the lower limit $\underline{P}_{DG}$ is set at zero for simplicity. Meanwhile, reactive power is always tightly coupled with and affected by the active power generation [34]. Fig. 5 shows the feasible regions of the power injections from WT and PV. Let us first look into the doubly-fed induction wind turbine. To model reactive power constraints, we take into consideration limits on both stator currents in the steady-state model. The corresponding upper $\bar{Q}_{WT}(i)$ and lower limits $\underline{Q}_{WT}(i)$ at bus i are described as

$$\bar{Q}_{WT}(i) = \sqrt{S_{WT}^2(i) - P_{WT}^2(i)} \tag{26}$$

$$\underline{Q}_{WT}(i) = Q_{WT}^{\min}(i) \tag{27}$$

As for a PV system, the capacity of the inverter and harmonic distortions mainly determine reactive power. Assume γ is the maximum power factor considering harmonic distortions, then the upper $\bar{Q}_{PV}(i)$ and lower $\underline{Q}_{PV}(i)$ limits of reactive power are described as

$$\bar{Q}_{PV}(i) = \min\left(\sqrt{S_{PV}^2(i) - P_{PV}^2(i)}, P_{PV}(i) \times \tan\gamma\right) \tag{28}$$

$$\underline{Q}_{PV}(i) = -\bar{Q}_{PV}(i) \tag{29}$$

2) Electric Storage System (ESS): ESS can take the role of balancing the power generated by DERs, and its charge/discharge power is optimally calculated at the economic dispatch stage. In our model, we consider the ESS as a negative load whose active power is known and its reactive power is determined by (26) and (29) [35]. The plug-in electric vehicles (PEVs) are quite different from traditional loads as PEVs would consume electricity and may have the vehicle to grid (V2G) function. In general, a PEV aggregator would manage PEVs within a certain region [30]. In the proposed hierarchical control structure, DSO would interact with aggregators rather than the owners of individual PEVs. Hence, in our model we assume a charging station is coupled with the inverter. It is regarded as a reactive power provider (see [36], [37]) whose reactive power is also constrained by (26) and (29).

The shunt capacitor bank settings are determined at the economic dispatch stage and q_i^{sc} is assumed constant in the presented model.

$$Q_{sc} = q_i^{sc} V_i^2 \tag{30}$$

The SVC is continuously adjusted, as it has better dynamic control performance, with constraints shown in (8) respected.

D. Modeling Loads

In APDS, both fixed and controllable loads are considered. The DSO's responsibility is to fully supply fixed loads by taking advantage of controllable loads so as to maximize the social welfare. The number of controllable loads (such as thermostatically controlled load) can be very large due to the rapid development of intelligent residential systems [38]. So it is important to take advantage of controllable loads in APDS for voltage control. In the proposed model, the nodal active and reactive loads represented by P_L and Q_L are determined by:

$$P_{cl} \le P_L \le P_{cl} + P_{fl} \tag{31}$$

$$Q_{cl} \le Q_L \le Q_{cl} + Q_{fl} \tag{32}$$

where P_{cl} and Q_{cl} are controllable active and reactive loads, respectively; P_{fl} and Q_{fl} are fixed active and reactive loads, respectively.

Algorithm 1 Parallelized Variable Updating Mechanism

1. *Update state variables*

$$(S_a^{k+1}, V_a^{k+1}) := \arg\min_{S_a, V_a}(F_a(S_a, V_a)+$$
$$(\rho/2) * (\|S_a - S_a^k + \bar{S}_a^k + u_a^k\|_2^2 + \|V_a - \bar{V}_a^k - \bar{n}_a^{k-1} + n_a^k\|_2^2)) \ a \in A$$

2. *Update dual variables*

$$u_j^{k+1} := \bar{u}_j^k + \bar{S}_j^{k+1} \ j \in J$$
$$n_j^{k+1} := \bar{n}_j^k + \bar{V}_j^{k+1} \ j \in J$$

V. ADMM-Based Solution Methodology

A. ADMM Algorithm

ADMM is an algorithm that possesses not only the decomposability of dual ascent but also the superior convergence properties of Lagrangian multipliers-based methods. Generally, ADMM solves optimization problems in the following form [39]:

$$\min \ f(x) + g(z) \tag{33a}$$
$$s.t. \ x - z = 0 \tag{33b}$$

where $x \in C$ and z is an artificial variable with the same dimension as x; g is the indicator function of C.

Accordingly, (P1) can be rewritten in the ADMM form as:

$$(\mathbf{P2}) \min \ \sum_{a\in A} F_a(S_a, V_a) + \sum_{j\in J}\left[g_j(\eta_j) + h_j(\zeta_j)\right] \tag{34a}$$
$$s.t. \ S = \eta, V = \zeta \tag{34b}$$
$$S \in \mathbf{S} \ and \ V \in \mathbf{V} \tag{34c}$$

where $g_j(\eta_j)$ and $h_j(\zeta_j)$ are the indicator functions, and artificial variables η and ζ have the same dimension as S and V, respectively. The indicator functions are given by

$$g_j(\eta_j) = \begin{cases} 0 & \eta_j \in \{\eta_j | \bar{\eta}_j = 0\} \\ +\infty & \eta_j \notin \{\eta_j | \bar{\eta}_j = 0\} \end{cases} \tag{35}$$

$$h_j(\zeta_j) = \begin{cases} 0 & \zeta_j \in \{\zeta_j | \tilde{\zeta}_j = 0\} \\ +\infty & \zeta_j \notin \{\zeta_j | \tilde{\zeta}_j = 0\} \end{cases} \tag{36}$$

The dual variables are scaled to $u = y_p/\rho$ and $n = y_\theta/\rho$, where ρ is the step size. The augmented Lagrangian function for (P2) can be written as

$$L_\rho = \sum_{a\in A} F_a(S_a, V_a) + \sum_{j\in J}\left[g_j(\eta_j) + h_j(\zeta_j)\right] + (\rho/2)\left(\|S - \eta + u\|_2^2 + \|V - \zeta + n\|_2^2\right) \tag{37}$$

The augmented Lagrangian function (37) can be decomposed in terms of each entity. The variables are updated at each iteration by eliminating artificial variables η and ζ, as illustrated in Algorithm 1.

B. Overall Solution Framework

The proposed ADMM algorithm can converge to a global optimum. The primal and dual residuals at the k-th iteration are represented by r^k and s^k as defined in [39] by

$$r^k = \left(\bar{S}^k, \tilde{V}^k\right) \ and \ s^k = \rho\left(\left(S^k - \bar{S}^k\right) - \left(S^{k-1} - \bar{S}^{k-1}\right), \bar{V}^k - \bar{V}^{k-1}\right) \tag{38}$$

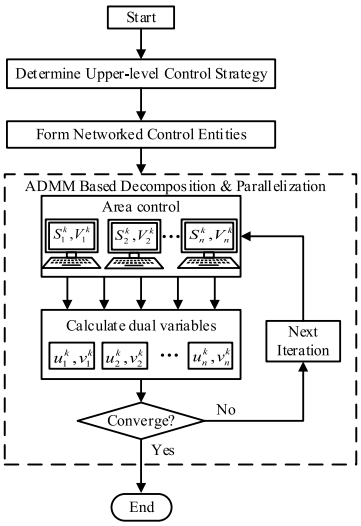

Fig. 6. Flowchart of optimal voltage control in APDS.

The following criterion is defined for checking convergence:

$$\left\|r^k\right\|_2 \le e^{pri} \ and \ \left\|s^k\right\|_2 \le e^{dual} \tag{39}$$

where e^{pri} and e^{dual} are primal and dual tolerances, respectively. Given the network size, the tolerance can be normalized to the absolute tolerance e^{abs} defined as

$$e^{abs} = e^{pri}/\sqrt{|T|} = e^{dual}/\sqrt{|T|} \tag{40}$$

where $|T|$ is the total number of terminals in APDS. The solution process is illustrated in Fig. 6.

As for the multi-area control architecture, the $(k+1)$th iteration of the objective function for one entity can be written as follows:

$$\min \ F = w_1/F_1^0 \sum_{(i,j)} r_{ij} \times l_{ij} + w_2/F_2^0 \sum_{i\in B}\left(\frac{v_i - v_i^{ref}}{\bar{V}_i^2 - \underline{V}_i^2}\right)^2 + (\rho/2)\left(\sum_{(i,j)}\left\|S_{ij} - S_{ij}^k + \bar{S}_{ij}^k + u_{ij}^k\right\|_2^2 + \sum_{i\in B}\left\|v_i - \bar{v}_i^k + \bar{n}_i^{k-1} - n_i^k\right\|_2^2\right) \tag{41}$$

$$s.t. \begin{cases} Eq.(5) - (10) \\ Eq.(12), (15) \\ Eq.(22) - (32) \end{cases} \tag{42}$$

which is a SOC problem that can be solved by MOSEK 7.0. Note that at each iteration, each entity will exchange the current primal solution with its neighbors. Then each entity updates the dual variables and checks whether or not the convergence criterion is met. If not, the iteration continues.

VI. Numerical Results

In this section, case studies on the modified IEEE 33-bus and 123-bus test systems are conducted to demonstrate the proposed voltage control strategy. Numerical experiments are implemented using MATLAB 2014 on a personal computer

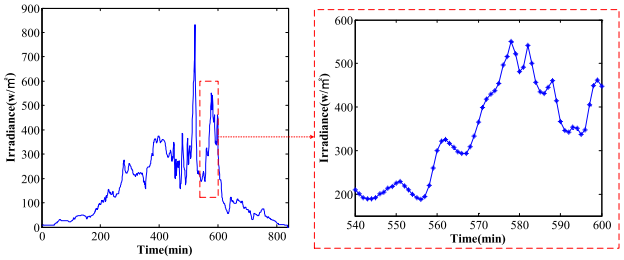

Fig. 7. Typical daily solar irradiance data.

with an Intel Core (i5, 3.20GHz) and 4GB memory. MOSEK 7.0 [40] is used to solve the SOCP problems, and IPOPT 3.12 [41] is employed to solve the conventional AC OPF problem.

Given that the PV is the dominant DER in the specified distribution systems, only variable PVs are considered in the test cases. Fig. 7 shows the solar irradiation collected on 16^{th} January 2016 at the University of Queensland [42], which lasts for about 800 minutes. We randomly select a one-hour period with one-minute discretization (i.e., [541, 600]) and assume that all installed PVs (each with a capacity of 150 kVA and a nominal power factor of 0.95) share the same solar irradiance. Constrained by the high investment cost, a single SVC with the capacity of [-100, 300] kVar is connected to bus 24 in the modified IEEE 33-bus system and bus 41 in the modified IEEE 123-bus system. The weights in the objective function are set at $w_1 = w_2 = 0.5$ since the selection of best weights is not the focus of this work. The pertinent data can be assessed at http://motor.ece.iit.edu/data/APDS.xls.

A. IEEE 33-Bus Test System

The original system data can be found in [43]. The total active and reactive loads are 3,635 kW and 2,265 kVar, respectively. Bus 1 with a voltage magnitude of 1.07 p.u. is connected to the distribution substation. 10 PV systems are installed at buses 2, 7, 8, 14, 16, 19, 23, 24, 26 and 30.

We apply the proposed voltage control strategy in order to maintain the bus voltage magnitudes within the pre-specified range of [0.95, 1.05] over the study period. The proposed strategy will be employed to prevent voltage violations as variable PV power outputs are utilized. Consider Fig. 8 which shows the representative voltage magnitude at bus 8 with the upper limit of 1.05 p.u. maintained during [571, 590] when the proposed method is applied. Fig. 8 also shows the voltage magnitude at bus 8 when no voltage control strategy is applied. In this case, the voltage magnitude exceeds the upper limit at [565,594], and this means APDS may suffer voltage problems resulting from DER variations.

Fig. 9 illustrates the PV power injections into three representative buses. The active power outputs of PVs at buses 2 and 24 follow the maximum-power-output mode where no curtailment would occur; while the active power output at bus 8 is restricted to zero at [571,590]. This is because the voltage magnitude at bus 8 would reach its upper limit during this time interval and any additional PV power injection will lead to voltage violations. The power factors at all PV systems

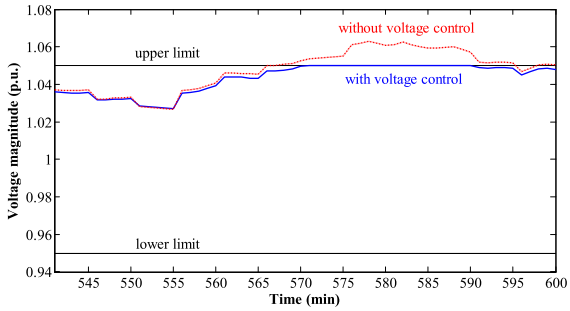

Fig. 8. Voltage magnitude at bus 8 in the IEEE 33-bus system.

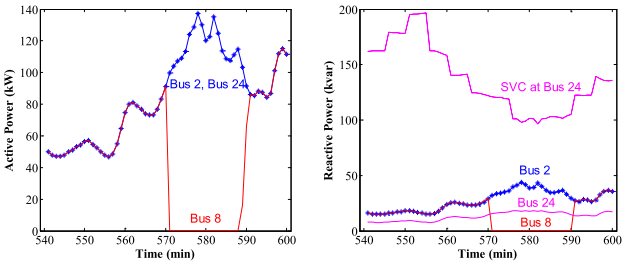

(a) Active power (b) Reactive power

Fig. 9. Power injections at representative buses in the IEEE 33-bus system.

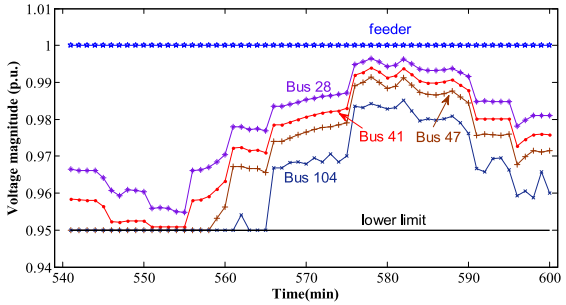

Fig. 10. Voltage magnitudes at representative buses in the IEEE 123-bus system.

conform to the nominal value except that at bus 24 which is connected to a SVC and displays a higher power factor.

B. IEEE 123-Bus Test System

The original system data can be found in [43] with load data and operating conditions available in [11]. Bus 1 having a voltage magnitude of 1.0 p.u. connects with the distribution substation. 10 PV systems are installed at different buses (i.e., buses 6, 28, 35, 37, 47, 48, 49, 65, 76 and 104).

Fig. 10 exhibits the voltage magnitudes at four representative buses, given that all bus voltages stay within the pre-specified range of [0.95, 1.05]. The voltage magnitude at bus 28 is relatively high as the local PV system effectively reduces the local load and thus abates the voltage drop. In comparison, bus 41 which carries a higher net load witnesses a lower voltage magnitude. In Fig. 11, the PV systems are operated in the maximum-power-output mode and the SVC at bus 41 produces reactive power following the load changes.

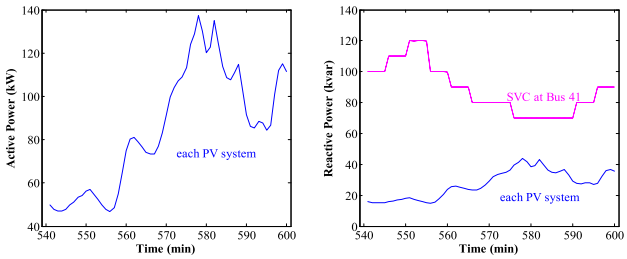

(a) Active power injections (b) Reactive power injections

Fig. 11. Power injections from PV systems in the IEEE 123-bus system.

TABLE I
COMPARISONS BETWEEN TWO MODES

Initial value ρ	IEEE 33-bus system iteration		IEEE 123-bus system iteration	
	fixed- ρ	varying- ρ	fixed- ρ	varying- ρ
0.01	501	20	204	114
0.1	53	39	97	112
0.5	24	24	71	71
1	30	30	104	104
10	not converge	54	not converge	157
100	not converge	59	not converge	161

C. Efficiency of the Proposed Algorithm

Appropriately choosing an optimal step size is an important matter as it has a significant impact on the convergence of the algorithm proposed. Here, a variable step size scheme [39] is applied. More specifically, the step size ρ varies at each iteration, in order to improve the convergence speed as well as make the convergence performance less dependent on the initial value. A simple updating scheme is shown as follows:

$$\rho^{k+1} := \begin{cases} \tau\rho^k & if \left\|r^k\right\|_2 > \mu\left\|s^k\right\|_2 \\ \rho^k/\tau & if \left\|s^k\right\|_2 > \mu\left\|r^k\right\|_2 \\ \rho^k & \text{otherwise} \end{cases} \tag{43}$$

where $\mu > 1$, $\tau > 1$. Here, set $\mu = 20$ and $\tau = 2$. Comparisons between the variable step size scheme and the fixed one are conducted to demonstrate the advantages of the variable one.

As can be seen in Table I that when the initial value of the step size is specified to be 10 or 100, the fixed step size scheme cannot converge to a global optimal solution, but the variable one is feasible for both test systems. In addition, when the step size is as small as 0.01, the variable step size scheme can greatly reduce the number of iterations regardless of 33-bus system or 123-bus system. Thus, the variable step size scheme is more robust than the fixed one.

The efficiency of the ADMM-based method is compared among three distinct network decomposition strategies:

1) Mode A (common case): geographically partition the network into distinct entities for decentralized optimization.

2) Mode B (extreme case): perform a component-wise partition where each entity is a single component for decentralized optimization.

3) Mode C (extreme case): treat the network as a single entity, which is the same as the centralized optimization.

TABLE II
COMPARISONS OF COMPUTATION TIME FOR IEEE 33-BUS SYSTEM

Mode	Control Entities	Iteration	Time/s
Mode A	**Entity 1:**{1 2 3 4 5 6 19 20 21 22 23 24 25}; **Entity 2:**{26 27 28 29 30 31 32 33}; **Entity 3:**{7 8 9 10 11 12 13 14 15 16 17 18}	24	0.334
Mode B	Each individual component forms an entity	362	0.471
Mode C	/	/	0.873

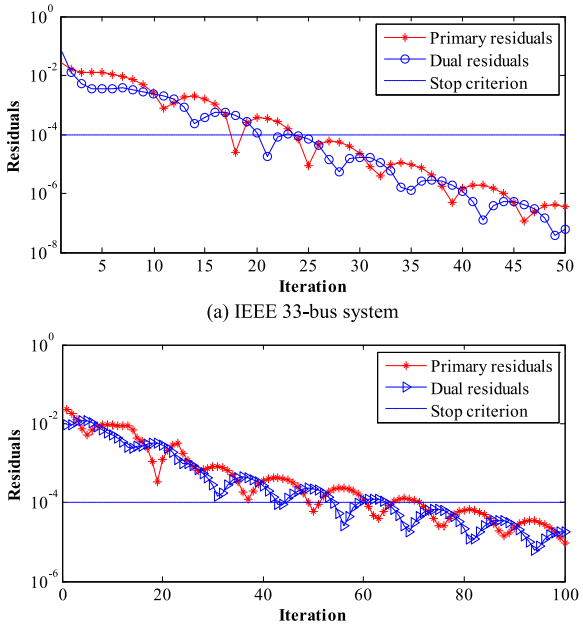

(a) IEEE 33-bus system

(b) IEEE 123-bus system

Fig. 12. Iteration process.

The absolute tolerance is set as 10^{-4}. The initial value of the step size is set as 0.5. Numerical results for IEEE 33-bus and 123-bus systems are listed in Tables II and III, respectively. All case studies are run on a single machine. Thus, to get the computation time when the model is implemented in a distributed manner, the longest time the entity takes is considered as the average time in each iteration process. Thus, the computation time does not include the elapsed time for communications among neighboring entities. Note that the computation time here is the time the solver consumes.

The close-form solution for each individual component in Mode B (see http://motor.ece.iit.edu/data/APDS.xls) is derived to speed up the computation time. In Mode B, the distribution line model takes more time than any other component and hence we take the corresponding computation time as the average time in each iteration process. As shown in Table II, Mode A has the least iteration number. Furthermore, Mode A offers more options as the number of APDS components grows. Fig. 12 shows the iteration process for Mode A in the two systems. More specifically, the ADMM algorithm converges in 24 and 71 iterations and consumes 0.334 and 0.923 seconds for IEEE 33-bus and 123-bus systems, respectively.

As we mainly focus on the convergence performance of the algorithm, the APDS bandwidth is assumed to be sufficient for meeting the communication requirements in the proposed strategy and thus the time latency is ignored. On one hand,

TABLE III
COMPARISONS OF COMPUTATION TIME FOR IEEE 123-BUS SYSTEM

Mode	Control Entities	Iteration	Time/s
Mode A	**Entity 1:** {1 123 2 3 4 5 6 7 8 9 10 11 12 13 14 34 15 16 17}; **Entity 2:** {18 19 20 21 22 23 24 25 26 27 28 29 30 122 31 32 33}; **Entity 3:** {121 35 36 37 38 39 40 41 42 43 44 45 46 47 48 49 50 51 116}; **Entity 4:** {115 108 109 110 111 112 113 114 105 106 107 101 102 103 104 117}; **Entity 5:** {120 52 53 54 55 56 57 58 59 60 119 67 68 69 70 71 97 98 99 100 118} **Entity 6:** {72 73 74 75 76 77 78 79 80 81 82 83 84 85 86 87 88 89 90 91 92 93 94 95 96}	71	0.923
Mode B	Each individual component forms an entity	601	0.793
Mode C	/	/	2.583

Table III shows that Mode B takes less time than Mode A for the 123-bus system. On the other hand, the communication delays are related to the iteration number. Hence, the time latency in Mode B will be more obvious in practical power systems comparing to Mode A and then influence the efficiency. In addition, Mode A allows for an expressive model, which can incorporate the intricate couplings among storage devices, loads and renewable energy resources.

D. Robust Performance

Assume that a random malfunction of the local controller at each junction occurs during the solution process thereby interrupting the broadcasting and gathering processes. We model the malfunction as a random packet drop. Specifically, each entity may fail to broadcast the information to (gather the information from) neighbor control entity with probability ρ. Here it is assumed that the control entity would use the information it got in last iteration if packet drops occur. As shown in Table IV, both modes can converge to the optimum solution when facing the random malfunction. More iterations will be demanded with a higher probability of communication failure. Comparing to Mode B, the iteration number does not change remarkably in Mode A regardless of the 33-bus system or 123-bus system when a malfunction occurs. Thus, Mode A has a better robust performance. This is mainly because Mode A needs less amount of information communication and hence tends to be more robust against the packet drops.

Additionally, the proposed control strategy could be robust against the frequent changes in the system condition caused by the use of plug and play devices. For instance, when a group of PEVs are suddenly integrated into APDS, the corresponding local controller will detect the power demand of PEVs and broadcast the information at the next iteration even without stopping and restarting the solution process.

E. Accuracy of SOC Relaxation

In order to demonstrate the accuracy of SOC relaxation after attaining the converged solution, the following evaluation index is defined:

$$d_{evi} = \left\| l_{ik} - \frac{P_{ik}^2 + Q_{ik}^2}{|V_i|^2} \right\|_\infty \tag{44}$$

TABLE IV
COMPARISONS OF ROBUST PERFORMANCE BETWEEN MODE A AND MODE B

Probability	Iteration for 33-bus		Iteration for 123-bus	
	Mode A	Mode B	Mode A	Mode B
0.1	25	529	73	646
0.2	27	651	86	813
0.3	32	899	88	871

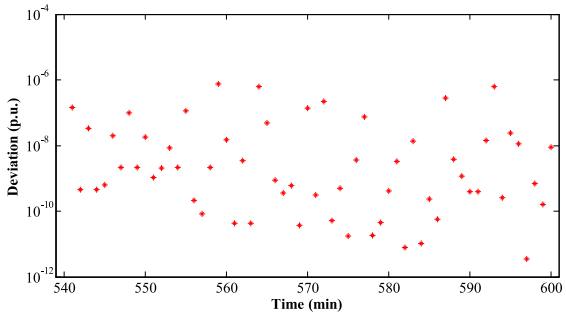

(a) IEEE 33-bus system

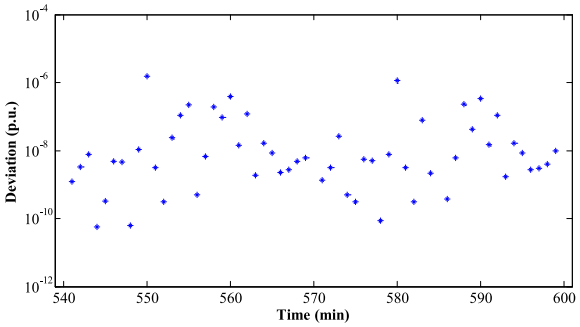

(b) IEEE 123-bus system

Fig. 13. SOC relaxation accuracy.

where d_{evi} represents the maximum deviation of the square of a branch current magnitude. Fig. 13 depicts all the evaluation results where the deviations are smaller than 10^{-6} and significantly smaller than the square of the current magnitude. Thus, the SOC relaxation is deemed exact. Compared with the conventional AC OPF problem (which requires 2.776 s in the centralized optimization mode to get a local optimum for IEEE 123-bus system), the use of SOC relaxation is faster and can lead to a theoretically global optimum, which is more desirable by DSO operators.

VII. CONCLUSION

In this work, a new distributed control method is developed to ensure voltage security in APDS. The original optimization model is relaxed into a SOC model and a distributed algorithm based on ADMM is employed to solve the convex problem which just requires exchanging messages among neighboring control entities. It is shown that the proposed method is effective in mitigating the voltage magnitude violations, and has good convergence and faster solution speed compared with the traditional centralized mode, as demonstrated by case studies on IEEE 33-bus and 123-bus systems. Additionally, the SOC relaxation is also verified to be exact. Comparing to

the centralized method, the proposed method has three advantages. Firstly, the proposed model can adapt to the increasing penetration of DERs as it can coordinate a large number of DERs in a decentralized way based on parallel computation. Secondly, the proposed method has a good self-healing capability as it is shown to be robust against the communication failures. By extension, it is also applicable when the system condition changes frequently caused by the use of plug and play devices. Thirdly, the centralized manner may suffer the risk of leaking the privacy of users. Conversely, the distributed manner can protect the privacy of users as the control entity in the proposed model only exchanges limited information with its neighboring control entities.

The proposed model is based on single-phase (more accurately, positive sequence) networks. However, distribution networks are commonly unbalanced three-phase ones. The presented model can be extended to unbalanced three-phase networks, and this represents our future efforts. We will extend the presented model to three-phase unbalanced distribution networks, and study the efficiency of the proposed method in large-scale distribution systems.

In addition, the area partition strategy is crucial to the algorithm efficiency. In Section II, two rules are employed to divide a distribution network into sub-networks according to the corresponding geographic and topology structures. We have also carried out several case studies (see http://motor.ece.iit.edu/data/APDS.xls) to study the effect of the area partition strategy on the algorithm efficiency. An index is constructed to evaluate the coupled degree among control areas. Simulation results show that when a distribution network is partitioned into a certain number of control areas, if the coupled degree is high, the number of demanded iterations will be less. Thus, how to divide a distribution network into several control entities reasonably is also our research topic.

REFERENCES

[1] J. Zhao *et al.*, "A review of active management for distribution networks: Current status and future development trends," *Elect. Power Compon. Syst.*, vol. 42, nos. 3–4, pp. 280–293, Mar. 2014.

[2] A. Keane, L. F. Ochoa, E. Vittal, C. J. Dent, and G. P. Harrison, "Enhanced utilization of voltage control resources with distributed generation," *IEEE Trans. Power Syst.*, vol. 26, no. 1, pp. 252–260, Feb. 2011.

[3] T. Ding, Q. Guo, H. Sun, B. Wang, and F. Xu, "A quadratic robust optimization model for automatic voltage control on wind farm side," in *Proc. IEEE Power Energy Soc. Gen. Meeting*, Vancouver, BC, Canada, 2013, pp. 1–5.

[4] S. Corsi, P. Marannino, N. Losignore, G. Moreschini, and G. Piccini, "Coordination between the reactive power scheduling function and the hierarchical voltage control of the EHV ENEL system," *IEEE Trans. Power Syst.*, vol. 10, no. 2, pp. 686–694, May 1995.

[5] T. Ding, R. Bo, H. Sun, F. Li, and Q. Guo, "A robust two-level coordinated static voltage security region for centrally integrated wind farms," *IEEE Trans. Smart Grid*, vol. 7, no. 1, pp. 460–470, Jan. 2016.

[6] A. G. Madureira and J. A. P. Lopes, "Coordinated voltage support in distribution networks with distributed generation and microgrids," *IET Renew. Power Gener.*, vol. 3, no. 4, pp. 439–454, Dec. 2009.

[7] R. A. F. Currie, G. W. Ault, C. E. T. Foote, and J. R. McDonald, "Active power-flow management utilising operating margins for the increased connection of distributed generation," *IET Gener. Transm. Distrib.*, vol. 1, no. 1, pp. 197–202, Jan. 2007.

[8] B. Zhang, A. Y. S. Lam, A. D. Domínguez-García, and D. Tse, "An optimal and distributed method for voltage regulation in power distribution systems," *IEEE Trans. Power Syst.*, vol. 30, no. 4, pp. 1714–1726, Jul. 2015.

[9] W. Sheng, K.-Y. Liu, and S. Cheng, "Optimal power flow algorithm and analysis in distribution system considering distributed generation," *IET Gener. Transm. Distrib.*, vol. 8, no. 2, pp. 261–272, Feb. 2014.

[10] R. Majumder, "Aspect of voltage stability and reactive power support in active distribution," *IET Gener. Transm. Distrib.*, vol. 8, no. 3, pp. 442–450, Mar. 2014.

[11] T. Ding, S. Liu, W. Yuan, Z. Bie, and B. Zeng, "A two-stage robust reactive power optimization considering uncertain wind power integration in active distribution networks," *IEEE Trans. Sustain. Energy*, vol. 7, no. 1, pp. 301–311, Jan. 2016.

[12] G. Valverade and T. V. Cutsem, "Model predictive control of voltages in active distribution networks," *IEEE Trans. Smart Grid*, vol. 4, no. 4, pp. 2152–2161, Dec. 2013.

[13] P. Juanuwattanakul and M. A. S. Masoum, "Increasing distributed generation penetration in multiphase distribution networks considering grid losses, maximum loading factor and bus voltage limits," *IET Gener. Transm. Distrib.*, vol. 6, no. 12, pp. 1262–1271, Dec. 2012.

[14] S. H. Low, "Convex relaxation of optimal power flow—Part I: Formulations and equivalence," *IEEE Trans. Control Netw. Syst.*, vol. 1, no. 1, pp. 15–27, Mar. 2014.

[15] M. Farivar and S. H. Low, "Branch flow model: Relaxations and convexification—Part I," *IEEE Trans. Power Syst.*, vol. 28, no. 3, pp. 2554–2564, Aug. 2013.

[16] W. Zheng, W. Wu, B. Zhang, H. Sun, and Y. Liu, "A fully distributed reactive power optimization and control method for active distribution networks," *IEEE Trans. Smart Grid*, vol. 7, no. 2, pp. 1021–1033, Mar. 2016.

[17] M. Farivar, R. Neal, C. Clarke, and S. Low, "Optimal inverter VAR control in distribution systems with high PV penetration," in *Proc. IEEE Power Energy Soc. Gen. Meeting*, San Diego, CA, USA, Jul. 2012, pp. 1–7.

[18] N. Li, L. Chen, and S. H. Low, "Exact convex relaxation of OPF for radial networks using branch flow model," in *Proc. IEEE 3rd Int. Conf. Smart Grid Commun. (SmartGridComm)*, Tainan, Taiwan, Nov. 2012, pp. 7–12.

[19] Z. Li, M. Shahidehpour, A. Alabdulwahab, and A. Abusorrah, "Bilevel model for analyzing coordinated cyber-physical attacks on power systems," *IEEE Trans. Smart Grid*, vol. 7, no. 5, pp. 2260–2272, Sep. 2016.

[20] H. Xin, Z. Lu, Z. Qu, D. Gan, and D. Qi, "Cooperative control strategy for multiple photovoltaic generators in distribution networks," *IET Control Theory*, vol. 5, no. 14, pp. 1617–1629, Sep. 2011.

[21] K. Tanaka *et al.*, "Decentralised control of voltage in distribution systems by distributed generators," *IET Gener. Transm. Distrib.*, vol. 4, no. 11, pp. 1251–1260, Nov. 2010.

[22] M. Zhu and S. Martinez, "On distributed convex optimization under inequality and equality constraints," *IEEE Trans. Autom. Control*, vol. 57, no. 1, pp. 151–164, Jan. 2012.

[23] H. Yang, D. Yi, J. Zhao, and Z. Dong, "Distributed optimal dispatch of virtual power plant via limited communication," *IEEE Trans. Power Syst.*, vol. 28, no. 3, pp. 3511–3512, Aug. 2013.

[24] Z. Li, W. Wu, B. Zeng, M. Shahidehpour, and B. Zhang, "Decentralized contingency-constrained tie-line scheduling for multi-area power grids," *IEEE Trans. Power Syst.*, vol. 32, no. 1, pp. 354–367, Jan. 2017.

[25] Z. Li *et al.*, "Decentralized multiarea robust generation unit and tie-line scheduling under wind power uncertainty," *IEEE Trans. Sustain. Energy*, vol. 6, no. 4, pp. 1377–1388, Oct. 2015.

[26] L. Gan and S. H. Low, "Convex relaxations and linear approximation for optimal power flow in multiphase radial network," in *Proc. 18th Power Syst. Comput. Conf. (PSCC)*, Wrocaw, Poland, 2014, pp. 1–9.

[27] Q. Peng and S. H. Low, "Distributed algorithm for optimal power flow on a radial network," in *Proc. 53rd IEEE Conf. Decis. Control*, Los Angeles, CA, USA, Dec. 2014, pp. 167–172.

[28] Q. Peng and S. H. Low. *Distributed Algorithm for Optimal Power Flow on Unbalanced Multiphase Distribution Network*. Accessed on Dec. 10, 2015. [Online]. Available: http://arxiv.org/pdf/1512.06482v1.pdf

[29] Z.-P. Wang, H. Fan, S.-F. Wang, and G.-M. Wang, "A bilevel programming model for the reactive power optimization," in *Proc. 7th Int. Power Eng. Conf. (IPEC)*, Singapore, Nov./Dec. 2005, pp. 1–214.

[30] W. Yao, J. Zhao, F. Wen, Y. Xue, and G. Ledwich, "A hierarchical decomposition approach for coordinated dispatch of plug-in electric vehicles," *IEEE Trans. Power Syst.*, vol. 28, no. 3, pp. 2768–2778, Aug. 2013.

[31] X. Wang, Y. Gong, and C. Jiang, "Regional carbon emission management based on probabilistic power flow with correlated stochastic variables," *IEEE Trans. Power Syst.*, vol. 30, no. 2, pp. 1094–1103, Mar. 2015.
[32] *American National Standard for Electric Power Systems and Equipment—Voltage Ratings (60 Hertz)*, ANSI Standard C84.1-2006, 2006.
[33] *Energy Management System Application Program Interface (EMS-API), Part303: Common Information Mode (CIM) SCADA*, IEC Standard Draft IEC 61970, 2003.
[34] A. R. Malekpour, P. Anil, and S. Das, "Inverter-based VAR control in low voltage distribution systems with rooftop solar PV," in *Proc. IEEE North Amer. Power Symp.*, Manhattan, KS, USA, Sep. 2013, pp. 1–5.
[35] A. Giannitrapani, S. Paoletti, A. Vicino, and D. Zarrilli, "Optimal allocation of energy storage systems for voltage control in LV distribution networks," *IEEE Trans. Smart Grid*, to be published, doi: 10.1109/TSG.2016.2602480.
[36] M. N. Mojdehi and P. Ghosh, "An on-demand compensation function for an EV as a reactive power service provider," *IEEE Trans. Veh. Technol.*, vol. 65, no. 6, pp. 4572–4583, Jun. 2016.
[37] M. Restrepo, J. Morris, M. Kazerani, and C. A. Canizares, "Modeling and testing of a bidirectional smart charger for distribution system EV integration," *IEEE Trans. Smart Grid*, to be published, doi: 10.1109/TSG.2016.2547178.
[38] S. Li, W. Zhang, J. Lian, and K. Kalsi, "Market-based coordination of thermostatically controlled loads—Part I: A mechanism design formulation," *IEEE Trans. Power Syst.*, vol. 31, no. 2, pp. 1170–1178, Mar. 2016.
[39] S. Boyd, N. Parikh, E. Chu, B. Peleato, and J. Eckstein, "Distributed optimization and statistical learning via the alternating direction method of multipliers," *Found. Trends Mach. Learn.*, vol. 3, no. 1, pp. 1–122, Jan. 2011.
[40] *MOSEK*. Accessed on Sep. 20, 2015. [Online]. Available: https://mosek.com
[41] A. Wächter and L. T. Biegler, "On the implementation of an interior-point filter line-search algorithm for large-scale nonlinear programming," *Math. Program.*, vol. 106, no. 1, pp. 25–57, Mar. 2006.
[42] *UQ SQLAR PV Data*. Accessed on Jan. 16, 2016. [Online]. Available: http://solar.uq.edu.au/
[43] (2010). *Distribution Test Feeder Working Group, Distribution Test Feeders*. [Online]. Available: http://ewh.ieee.org/soc/pes/dsacom/testfeeders/index.html

Changsen Feng received the B.S. degree in electrical engineering from Shandong University, Jinan, China, in 2013. He is currently pursuing the Ph.D. degree in electrical engineering with the School of Electrical Engineering, Zhejiang University, Hangzhou, China. His research interest is optimization in power system.

Zhiyi Li (GS'14) received the B.S. degree in electrical engineering from Xi'an Jiaotong University, Xi'an, China, in 2011, and the M.E. degree in electrical engineering from Zhejiang University, Hangzhou, China, in 2014. He is currently pursuing the Ph.D. degree with the Department of Electrical and Computer Engineering, Illinois Institute of Technology, Chicago, IL, USA. His current research interests include cyber-physical power system and power system optimization.

Mohammad Shahidehpour (F'01) is the Bodine Distinguished Professor and the Chair with the Electrical and Computer Engineering Department, Illinois Institute of Technology, Chicago. He is also a Research Professor with the King Abdulaziz University, Saudi Arabia. He is a member of the U.S. National Academy of Engineering.

Fushuan Wen received the B.E. and M.E. degrees in electrical engineering from Tianjin University, Tianjin, China, in 1985 and 1988, respectively, and the Ph.D. degree from Zhejiang University, Hangzhou, China, in 1991.

He joined the Faculty of Zhejiang University in 1991, and has been a Full Professor and the Director of the Institute of Power Economics and Information since 1997, and the Director of Zhejiang University-Insigma Joint Research Center for Smart Grids since 2010. He had been a University Distinguished Professor, the Deputy Dean of the School of Electrical Engineering and the Director of the Institute of Power Economics and Electricity Markets, South China University of Technology, Guangzhou, China, from 2005 to 2009. Since 2014, he has been a Professor with the Universiti Teknologi Brunei (Brunei University of Technology), Brunei, on leave from Zhejiang University. His research interests include power industry restructuring, power system alarm processing, fault diagnosis and restoration strategies, and smart grids and electric vehicles.

Prof. Wen is an Editor of the IEEE TRANSACTIONS ON POWER SYSTEMS and the *IEEE Power Engineering Letters*, an Associate Editor of the *IET Generation, Transmission and Distribution*, the *Journal of Energy Engineering*, and the *Journal of Modern Power Systems and Clean Energy* (Springer).

Weijia Liu received the B.E. and Ph.D. degrees in electrical engineering from Zhejiang University, Hangzhou, China, in 2011 and 2016, respectively. He was a Project Assistant with the Department of Electrical Engineering, Hong Kong Polytechnic University, Hong Kong, from 2012 to 2013. His main research interests are power system restoration and smart grids.

Xiaolei Wang received the B.S. degree from Wuhan University, Wuhan, China, in 2013, and the M.E. degree from Zhejiang University, Hangzhou, China, in 2016, both in electrical engineering. She is currently with the Suzhou Power Supply Company, State Grid Corporation of China. Her main research interests include electric vehicles and optimization in power systems.